Indian Journal of Biochemistry & Biophysics
Vol. 63, September 2026, pp. 1047-1061
DOI: 10.56042/ijbb.v63i9.26776

Computational and experimental studies supporting the anti-breast cancer potential of N-hydroxyphthalimide

Karthik Nallasamy[1], Sumathi Sivaraman[1], Manu Vashishtha[2] & Jeyavijayan Subbiah[1,3]*

[1]Department of Physics, Kalasalingam Academy of Research and Education, Krishnankoil-626 126, Tamil Nadu, India

[2]Department of Chemistry, Dr. B. R. Ambedkar Institute of Technology, Port Blair, South Andaman-744 103, Andaman and Nicobar Islands, India

[3]Department of Physics, School of Engineering and Technology (SET), Dhanalakshmi Srinivasan University, Perambalur-621 212, Tamil Nadu, India

Received 21 December 2025; *revised 23 June 2026*

Breast cancer remains a major health challenge, creating a need for safer and more effective therapeutic agents. Therefore, the present study explores the structural, spectroscopic, and anti-breast cancer potential of N-Hydroxyphthalimide (NHP) using combined computational and experimental approaches. The molecular structure was optimized, and vibrational modes, electronic transitions, reactive sites, atomic charges, and frontier molecular orbitals (FMOs) were examined using density functional theory (DFT). Theoretical infrared, Raman, and UV-visible spectra exhibited good contract with experimental data. Hirshfeld surface investigation further clarified the nature of interactions and molecular bonding. *In silico* ADMET and Physicochemical profiling indicated favourable drug-likeness and bioavailability for NHP. Molecular docking studies revealed significant binding affinities against four breast cancer related proteins, with the highest binding affinity observed for 7KBS (-7.1 kcal/mol). Molecular dynamics (MD) simulations were run for 100 ns in order to verify the stability of the 7KBS-NHP complex. *In vitro* cytotoxicity assays using the MTT method demonstrated strong activity of NHP against MCF-7 and MDA-MB-231 cell lines, with IC_{50} values of 14.50 µg/mL and 16.90 µg/mL, respectively.

Keywords: Density functional theory (DFT), Frontier molecular orbitals (FMOs), Human intestinal absorption (HIA), N-Hydroxyphthalimide (NHP), Phthalimide derivative

Worldwide, breast cancer (BC) is the leading cause of cancer-related mortality among women, and its incidence rates have risen rapidly in recent years[1]. It happens due to cell genetic damage leading to changes and abnormal growth. Based on genetic and tissue research, this hormone influenced cancer is divided into three main types such as those that express human epidermal receptor 2 (HER2-), those that express hormone receptors (HR+ or ER+), and triple-negative breast cancer (TNBC) (ER−, PR−, HER2−)[2,3]. Regarding the precise mechanisms causing BC, there is a lot of uncertainty. The most popular type is hormone receptor positive BC, which mostly affects postmenopausal women and accounts for 60-70% of cases in wealthy nations[4]. Phthalimide is a pharmacophore scaffold that has been identified by an isoindoline-1,3-dione core that has an imide ring. Its hydrophobicity, which enables it to pass through biological membranes more easily *in vivo*, is one of the chemical characteristics that affect its biological activity. It also has an electron-donating group, an aromatic hydrophobic region, and a hydrogen bonding subunit[5]. Currently, thalidomide and pomalidomide, two phthalimide based derivatives, are used as second generation immunomodulatory drugs to treat Kaposi's sarcoma and multiple myeloma[6]. Over the past few years, phthalimide derivatives have been synthesized and thoroughly investigated for their potential as therapies for an extensive range of illnesses. Several biological effects, including anti-cancer, anti-epileptic, anti-psychotic, anti-platelet, anti-bacterial, anti-inflammatory, anti-fungal, anti-mycobacterial, anti-parasitic, anti-Alzheimer's, anti-viral, and anti-diabetic properties, have been demonstrated for these compounds[7].

In the majority of cases, this concern is valid, since it is well known that N-hydroxy metabolites of branded drugs can generate highly reactive species that can lead to serious side effects. However, this hazardous reactivity of N-OH groups usually occurs when the nitrogen atom is not part of a ring system. When the nitrogen atom is incorporated into an aromatic

*Correspondence:
E-mail: sjeyavijayan@gmail.com
Suppl. data available on respective page of NOPR

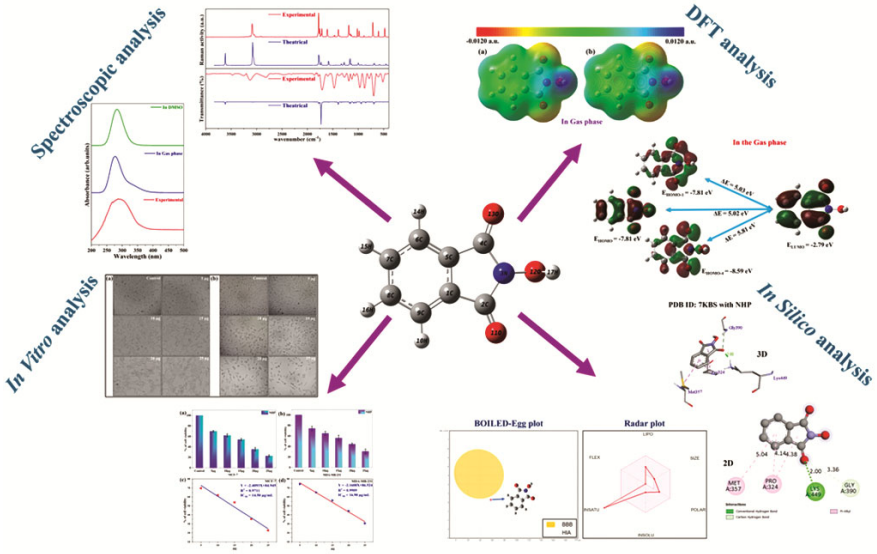

Graphical abstract

heterocyclic scaffold, however, the same sort of metabolic reactivity and associated toxicity is not expected[8]. However, the normal coordinate calculations were performed using the classical method developed by Krishnakumar *et al.*[9] for vibrational analysis. More recently, several kinds of N-hydroxy derivatives integrated into aromatic heterocyclic moieties have been shown in theoretical and experimental investigations to exhibit acceptable pharmacological properties. Furthermore, "NHF-derived carbon dots: a prevalidation approach in breast cancer treatment" was presented by Tiron *et al*[10]. In another related investigation, Wang *et al.*[11] reported that N-hydroxyphthalimide exhibits significant antitumor activity by suppressing the mTOR signaling pathway in BT-20 and LoVo cells. An extensive review of the literature indicates that N-hydroxyphthalimide (NHP) has not yet been explored using advanced methodologies such as DFT, molecular docking, ADMET profiling, or cytotoxicity assays. Considering the breast cancer risk highlighted earlier, along with the established significance of phthalimide derivatives and the functional relevance of the N-hydroxy group, the present study focuses on NHP. This compound was systematically examined using both computational and experimental approaches.

Materials and Method

Physical measurements

NHP was acquired through Sigma Aldrich in India with a grade of 97%. A Shimadzu IR Tracer-100 spectrometer was used to record the infrared spectra. The FT-Raman spectrum was measured using a Bruker RFS 27 standalone FT-Raman spectrometer with a resolution of 2 cm^{-1}. The wavenumber range that was used to record both spectra was 4000-400 cm^{-1}. The UV-Vis spectra of NHP in the 200-500 nm wavelength range were recorded using a UV-Vis spectrophotometer (UV-3501).

Computational method

The quantum chemical properties of NHP have been determined via DFT. All DFT calculations and visualizations are performed using the Gaussian 09W[12] and Gauss View 05[13] software packages. The DFT calculations in gas and DMSO phases were carried out using the 6-311++G(d,p) basis set and the B3LYP functional[14,15]. This study also examined the effects of the solvent, DMSO, on the electron's properties using the TD-DFT method. Electronic absorption spectra, HOMO-LUMO energies, thermodynamic properties, structural characteristics and Mulliken atomic charges have all been discussed. The vibrational assignments and absorption spectra were computed using the same level of basis set and compared with the experimental results for NHP. Potential Energy Distribution (PED) have been examined using the VEDA program[16]. The interactions between NHP have been examined using Hirshfeld surface analysis and fingerprint plots produced by the CrystalExplorer 17.0 software[17]. The pkCSM and SwissADME web server to quickly assess a range of pharmacokinetic parameters, ADMET characteristics, drug-likeness, the BOILED-Egg model, and the bioavailability radar[18]. PyRx tools

have been applied for molecular docking against the target proteins, and Discovery Studio was used to view the docked interactions[19,20]. Amber 22 was used to perform 100 ns molecular dynamics simulations[21] under NPT conditions using the ff14SB force field for proteins and GAFF for ligands. The systems were solvated with the explicit TIP3P water model, and the stability of the complexes was evaluated using root mean square deviation (RMSD), root mean square fluctuation (RMSF), solvent-accessible surface area (SASA), radius of gyration (R_g), and molecular mechanics generalized Born surface area (MM-GBSA) analyses.

Cytotoxicity evaluation using MTT assay

The breast cancer cell lines MDA-MB-231 and MCF-7 have been acquired from the National Centre for Cell Sciences (NCCS), Pune. Analytical grade reagents were purchased from HiMedia, chemicals such as MTT, DMSO, trypsin-EDTA, EDTA, Triton X-100, and related reagents were obtained from Sigma-Aldrich. The MTT experiment was conducted using Mosmann's technique[22] to evaluate cytotoxicity. Following a 24 h incubation period, cells were seeded in 96-well plates (1×10^4 cells/well) and treated with varying concentrations of NHP (5-25 µg/mL). Resulting treatment, four hours of incubation were spent with the addition of MTT (5 mg/mL). DMSO was used to dissolve the purple formazan crystals that were created when the mitochondrial enzymes of living cells reduced MTT. After that, absorbance at 540 nm was measured using a microplate reader. The dose response curve was used to determine the IC_{50} values, and each test was performed in triplicate, with at least three repetitions to ensure statistical correctness.

Results and Discussion

Molecular optimization of NHP

The NHP molecule structure was optimized with the 6-311++G(d,p) basis set and DFT/B3LYP method. This level of method is commonly used to investigate organic compounds because it achieves a perfect balance between computing accuracy and productivity. The NHP compound's optimized molecular structure is shown in (Fig. 1, and Table 1) lists the bond length and angle values in comparison with the experimental findings. Optimal molecular geometry was calculated for both gas and DMSO solvent phases. DMSO was chosen as the solvent

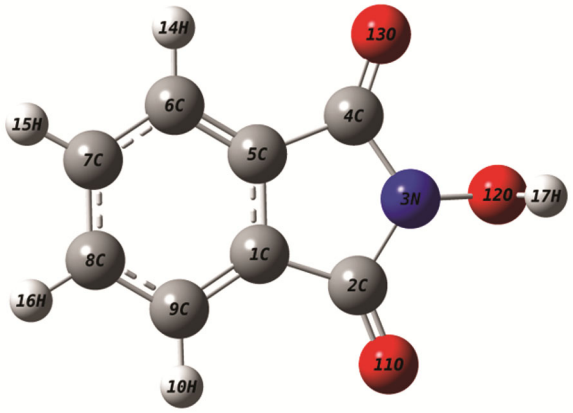

Fig. 1 — Optimized structure of N-Hydroxyphthalimide

Table 1 — The optimized structural parameters of N-Hydroxyphthalimide

Structural parameters			
Bond length (Å)	DFT-B3LYP/6-311++G(d,p)		Experimental[23]
	In the gas phase	In DMSO	
C1-C2	1.49	1.49	1.50
C1-C5	1.40	1.40	1.40
C1-C9	1.39	1.38	1.37
C2-N3	1.41	1.41	1.39
C2-O11	1.20	1.21	1.21
N3-C4	1.41	1.41	1.40
N3-O12	1.37	1.37	1.37
C4-C5	1.49	1.49	1.47
C4-O13	1.20	1.21	1.22
C5-C6	1.39	1.38	1.39
C6-C7	1.40	1.40	1.38
C6-H14	1.08	1.08	0.93
C7-C8	1.40	1.40	1.40
C7-H15	1.08	1.08	0.93
C8-C9	1.40	1.40	1.41
C8-H16	1.08	1.08	0.93
C9-H10	1.08	1.08	0.93
O12-H17	0.97	0.97	0.93
Bond angle (°)			
C2-C1-C5	109.0	108.8	108.0
C2-C1-C9	129.6	129.8	131.0
C5-C1-C9	121.4	121.4	121.0
C1-C2-N3	104.0	104.2	104.8
C1-C2-O11	130.2	130.5	130.2
N3-C2-O11	125.8	125.3	124.9
C2-N3-C4	113.7	113.6	113.4
C2-N3-O12	121.3	121.8	121.5
C4-N3-O12	121.3	121.8	123.3
N3-C4-C5	104.0	104.2	104.8
N3-C4-O13	125.8	125.3	124.6

(*Contd.*)

Table 1 — The optimized structural parameters of N-Hydroxyphthalimide (*Contd.*)

Structural parameters			
Bond angle (Å)	DFT-B3LYP/6-311++G(d,p)		Experimental [23]
	In the gas phase	In DMSO	
C5-C4-O13	130.2	130.5	130.6
C1-C5-C4	109.0	108.8	108.8
C1-C5-C6	121.4	121.4	121.0
C4-C5-C6	129.6	129.8	130.2
C5-C6-C7	117.5	117.5	118.3
C5-C6-H14	120.9	121.3	121.1
C7-C6-H14	121.6	121.2	121.1
C6-C7-C8	121.1	121.1	120.2
C6-C7-H15	119.6	119.5	119.1
C8-C7-H15	119.4	119.4	119.1
C7-C8-C9	121.1	121.1	122.0
C7-C8-H16	119.4	119.4	119.1
C9-C8-H16	119.6	119.5	119.1
C1-C9-C8	117.5	117.5	117.5
C1-C9-H10	120.9	121.3	120.8
C8-C9-H10	121.6	121.2	120.8
N3-O12-H17	106.1	106.2	112.4

model because of its high polarity and dielectric constant, which successfully account for solvent-solute interactions and offer a more accurate depiction of the molecular environment in the DFT calculations. The shortest bond length was identified between the carbon and hydrogen atoms C9-H17, with a value of 0.97 Å in both phases. This theoretical value shows a slight overestimation compared to the experimentally determined[23] bond length of 0.93 Å, indicating a minor deviation in hydrogen positioning in the computational model. In contrast, the longest bond lengths were observed between the carbon-carbon atoms C1-C2 and C4-C5, each calculated at 1.49 Å in both phases. The experimental data closely align with these values, reporting bond lengths of 1.50 Å for C1-C2 and 1.47 Å for C4-C5, respectively.

Concerning bond angles, the DFT calculations revealed the smallest angle between atoms C1-C2-N3 and N3-C4-C5, both computed as 104.0º in the gas phase and slightly increased to 104.2° in the DMSO phase. These are marginally lower than the experimental bond angle of 104.8°, indicating an understated solvent effect on molecular conformation. Conversely, the largest bond angles were found between C1-C2-O11 and C5-C4-O13, calculated as 130.2° in gas and 130.5° in DMSO phases. These computed values show strong reliability with the observed values of 130.2° for C1-C2-O11 and 130.6° for C5-C4-O13, demonstrating the reliability of the DFT method in predicting geometrical parameters. Other bond length and angle values are represented in (Table 1). Overall, there is good agreement between theoretical predictions and crystallographic measurements[23]. However, the minor discrepancies observed between computed and observed values may be attributed to differences in environmental conditions and limitations inherent in the computational model.

When NHP's thermodynamic characteristics are calculated in both gas phase and DMSO solvent, solvation effects cause small but significant variations. More stabilization from solvent-solute interactions, especially hydrogen bonding and dipole-dipole forces present in the polar DMSO medium, is indicated by the optimized global minimum energy being marginally more negative in DMSO (-369245.5971 kcal mol^{-1}) than in the gas phase (-369236.3036 kcal mol^{-1}). There are relatively few differences between phases in the values of total thermal energy and heat capacity, indicating that solvation has minimal impact on the internal vibrational modes and the thermal population of energy levels. It is possible to explain the slight decrease in vibrational entropy (from 23.042 to 22.648 cal mol^{-1} K^{-1}) and overall entropy (from 94.516 to 94.121 cal mol^{-1} K^{-1}) in DMSO to the decrease in vibrational motion in the condensed phase as a result of solute-solvent interactions and the limited molecular flexibility. The stabilization of polar conformers in the presence of a polar solvent is consistent with the dipole moment's notable increase from 3.981 Debye (gas) to 5.386 Debye (DMSO). The other parameters are shown in (Table 2).

Vibrational assignment

DFT vibrational analysis is a fundamental computational method for investigating the dynamics of molecular vibrations. The NHP has been projected to have 45 vibrational modes, comprising 13 in-plane, 13 out-of-plane, and 1 butterfly vibration, all of which are IR and Raman active, because it contains 17 atoms with 84 electrons. Spectra show that these vibrational modes are active since the optimized structure shows C1 symmetry. Using the VEDA tool, vibrational frequencies were computed at the same level of basis set, scaled by a factor of 0.9613, and assigned based on FT-IR and FT-Raman spectra obtained experimentally[24]. The vibrational

Table 2 — The thermodynamic parameters of N-Hydroxyphthalimide

Parameters	DFT-B3LYP/6-311++G(d,p)	
	In the gas phase	In DMSO
Optimized global minimum Energy (kcal mol^{-1})	-369236.3036	-369245.5971
Total energy(thermal), E_{total} (kcal mol^{-1})	80.444	80.363
Heat capacity, C_v (cal mol^{-1} k^{-1})	35.669	35.571
Total Entropy, S (cal mol^{-1} k^{-1})	94.516	94.121
Translational Entropy (cal mol^{-1} k^{-1})	41.175	41.175
Rotational Entropy (cal mol^{-1} k^{-1})	30.299	30.297
Vibrational Entropy (cal mol^{-1} k^{-1})	23.042	22.648
Vibrational energy, E_{vib} (kcal mol^{-1})	78.666	78.585
Zero-point vibrational energy, (kcal mol^{-1})	74.581	74.554
Rotational constants (GHz)		
A	1.730	1.736
B	0.864	0.863
C	0.578	0.578
Dipole moment (Debye)	3.981	5.386

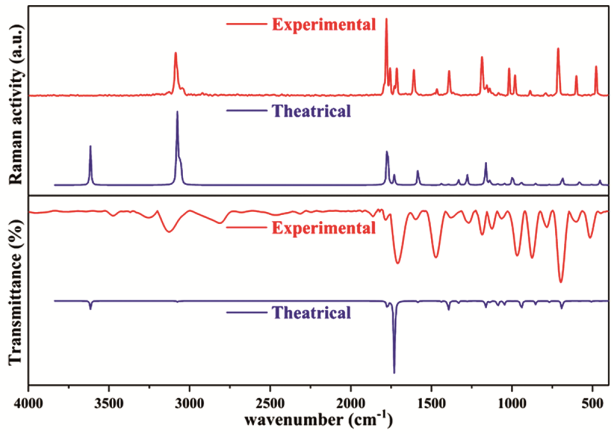

Fig. 2 — FT-IR and FT-Raman spectra of N-Hydroxyphthalimide

assignments are listed in (Suppl. Table S1). The FT-IR and FT-Raman spectra are shown in (Fig. 2). The theoretical calculations predict that the stretching mode of the OH group appears as distinct infrared bands in higher wavenumber regions.

The vibrations that are generated by the O-H, C=O, and N-O groups are categorized as stretching (υ), in-plane bending (b), and out-of-plane bending (ω). As the most sensitive vibrations, the O-H group vibrations show observable changes in the spectra of the hydrogen bonded species. The usual range for sharp O-H stretching[25] vibrations is 3200-3550 cm^{-1}.

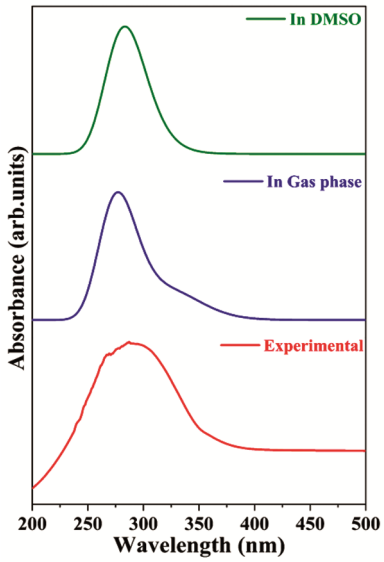

Fig. 3 — UV-Vis spectra of N-Hydroxyphthalimide in the experimental, DMSO and gas phase

The stretching vibration of the hydroxyl group, however, is shown to be active in the FT-IR and inactive in the FT-Raman spectrum in the current study. This vibration is anticipated to occur at 3615 cm^{-1} based on the scaled computational findings, and the observed wavenumber corresponds to this at 3490 cm^{-1}. The O-H group exhibits an in-plane bending vibration at 1130 cm^{-1} and 1139 cm^{-1} in both the Raman and infrared spectra, with a scaled value of 1136 cm^{-1}. It is expected that the out-of-plane bending mode occurs around 292 cm^{-1}.

In this study, the strong and weak bands seen at 1779 and 1720 cm^{-1} in the Raman and at 1783 and 1715 cm^{-1} in the IR spectrum have been assigned to C=O stretching vibrations (υC=O). The calculated spectra corresponding to these modes are 1773 and 1729 cm^{-1}. In the Raman spectra, N-O stretching vibration is also detected at 1460 cm^{-1}; their corresponding estimated wavenumber is 1438 cm^{-1}. All additional vibrational modes, both computed and theoretical, are included in (Suppl. Table S1) and exhibit strong agreement with the findings of the experiment.

UV-Vis and Frontier molecular orbital (FMO) analysis

UV-Vis spectroscopy was utilized to investigate the compound's electronic transitions, both theoretically and experimentally. This approach is critical for molecular structure studies, particularly in natural products and compounds with aromatic rings or heteroatoms[26]. Figure 3 shows the combined

Table 3 — Molecular orbital contributions of N-Hydroxyphthalimide

TD-DFT/ B3LYP/6-311++G(d,p) In the gas phase					Experimental wavelength (nm)
Energy (eV)	Oscillator strength	Computed wavelength (nm)	Major contributions	Assignment	
3.7714	0.0001	328.74	H-1→L (97 %)	π→π*	285.95
4.1579	0.0000	298.19	H→L (96 %)	π→π*	
4.4785	0.0005	276.84	H-4→L (83 %)	π→π*	
		In DMSO			
3.9266	0.0002	315.75	H-2→L (96 %)	π→π*	
3.9952	0.0023	310.34	H→L (96 %)	π→π*	
4.3805	0.0843	283.04	H-1→L (85 %)	π→π*	

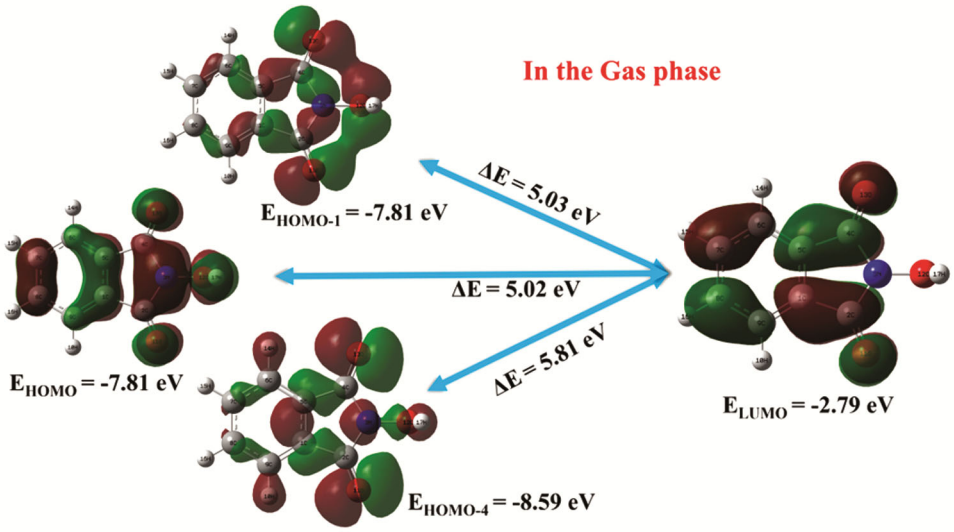

Fig. 4 — Molecular orbital energies for N-Hydroxyphthalimide in the gas phase

computational and experimental UV-Vis absorption spectra of NHP, while (Table 3) summarises the related excitation energy, oscillator strengths, and absorption wavelengths. In the experimental spectrum, the absorption peaks are observed at 285.95 nm. The computed absorption wavelength is found to be 328.74 nm (H-1→L (97 %)), 298.19 nm (H→L (96 %)), and 276.84 nm (H-4→L (83 %)) for the gas phase, and 315.75 nm (H-2→L (96 %)), 310.34 nm (H→L (96 %)), and 283.04 nm (H-1→L (85 %)) for the DMSO phase are related to π→π* transitions. The calculated absorption maxima at 276.84 nm (gas phase) and 283.04 nm (DMSO phase) show good agreement with the experimentally observed values. This correlation can be attributed to the fact that the corresponding transitions exhibit higher oscillator strengths and excitation energies compared to other possible transitions, indicating a stronger probability of electronic excitation at these Wavelengths.

Frontier molecular orbitals (FMOs) provide a better understanding of the observed UV-Vis transitions and the compound's chemical properties. The energy gap (ΔE) between HOMO and LUMO is an essential parameter in determining a molecule's kinetic stability and reactivity. A smaller HOMO-LUMO gap (ΔE) is often associated with higher chemical reactivity and lower kinetic stability, whereas a larger gap suggests greater stability and lower reactivity[26]. In this study, molecular orbitals were calculated at the same level of theory and considered for analysis, as illustrated in (Figs. 4 and Suppl. Fig. S1). As shown in Suppl. Table S2, the calculated energy gap values are 5.03 eV (H-1→L), 5.02 eV (H→L), and 5.81 eV (H-4→L) in the gas phase, and 5.20 eV (H-2→L), 4.86 eV (H→L), and 5.07 eV (H-1→L) in DMSO. These gaps, being close to 5 eV in both phases, indicate high molecular stability and reduced chemical reactivity, which are responsible for its biological activity. The hydroxyl group (OH) and the phthalimide core structure

possess the highest electron densities in the HOMO region, indicating that these are the main electron-donating sites. Upon transition to the LUMO, the electron density shifts away from the OH group and becomes concentrated on other parts of the molecule, particularly the conjugated π-systems, in both gas and DMSO phases, as shown in (Figs. 4 and Suppl. Fig. S1). This redistribution highlights a distinct intramolecular charge transfer pathway, suggesting that the OH group has a major role in the initial electron donation.

The calculated ionization potential (7.68 eV to 8.59 eV in both phases) of the molecule falls within the typical range for organic compounds, indicating moderate stability against electron loss and oxidation. Its relatively high electron affinity (2.79 eV to 2.82 eV in both phases) suggests a strong ability to accept electrons, enhancing its potential as an electrophile. The global hardness values (2.43 eV to 2.90 eV in both phases) classify the NHP as relatively hard, meaning it is chemically stable but less reactive, a fact further supported by the low global softness (0.17 eV^{-1} to 0.21 eV^{-1} in both phases). The electronegativity (5.25 eV to 5.69 eV in both phases) and chemical potential (-5.25 eV to -5.69 eV in both phases) values confirm a significant tendency to attract and tightly hold electrons, indicating high molecular stability. Finally, the global electrophilicity index (5.58 eV to 5.67 eV in both phases) is notably high, implying a strong electrophilic nature that may favour interactions with electron-rich biological targets. This combination of descriptors suggests the molecule is stable yet strongly electrophilic, capable of effective binding to nucleophilic sites, valuable for biological and anticancer applications, although its high hardness may limit its redox reactivity.

MEP and Mulliken charge analysis

MEP maps provide a three-dimensional representation of a molecule's electrostatic potential and illustrate its probable charge distribution using different color codes. Areas of highest positive electrostatic potential, which are highly susceptible to nucleophilic assaults, are typically represented by blue regions, whereas areas of maximum negative potential, which are vulnerable to electrophilic attacks, are represented by red regions[27]. Based on electrostatic potential values ranging from -0.120 e0 to +0.120 e0 in the gas phase (Fig. 5) and -0.121 e0 to +0.121 e0 in the DMSO phase (Suppl. Fig. S2), the MEP map of NHP has been generated in this work. In the DMSO phase, the comparable potential values were -0.07661 a.u. and -0.07443 a.u., centred on the C=O group, whereas the highest negative locations were found at -0.07156 a.u. and -0.07102 a.u. in the gas phase. Due to resonance stabilization and concentrated lone pairs, this strongly electronegative area indicates a considerable susceptibility to electrophilic attack. On the other hand, the hydrogen atom H17 was surrounded by the largest positive areas of electrostatic potential, with values of around +0.11778 a.u. in the gas phase and +0.11928 a.u. in the DMSO phase. This is equivalent to the terminal -OH group's hydrogen atom, whose high positive potential suggests a significant tendency for nucleophilic contact, particularly through hydrogen bonding in biological or intermolecular settings.

The same level of basis set was used for Mulliken atomic charges in the instance of NHP. The findings, which are shown in (Table 4), demonstrate how the

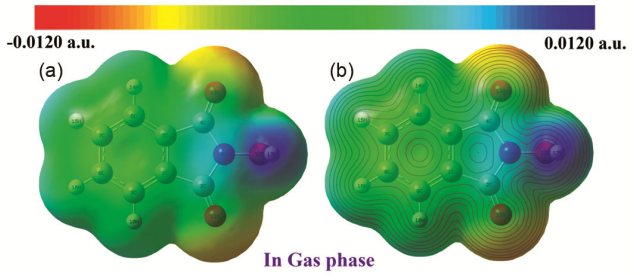

Fig. 5 — (a) Molecular Electrostatic potential and (b) Contours with electrostatic potential surface in the gas phase for N-Hydroxyphthalimide

Table 4 — Mulliken atomic charge for N-Hydroxyphthalimide

Atoms	Atomic Charges (Mulliken) by B3LYP/6-311++G(d,p)	
	In the gas phase	In DMSO
C1	0.40	0.41
C2	0.28	0.32
N3	-0.36	-0.31
C4	0.28	0.32
C5	0.40	0.41
C6	-0.62	-0.63
C7	-0.13	-0.17
C8	-0.13	-0.17
C9	-0.62	-0.63
H10	0.19	0.20
O11	-0.28	-0.36
O12	0.05	0.00
O13	-0.28	-0.36
H14	0.19	0.20
H15	0.18	0.21
H16	0.18	0.21
H17	0.28	0.32

atomic charges are distributed throughout the molecule. The carbon atoms C1 and C5 have the highest positive charge, measuring 0.40 in the gas phase and 0.41 in the DMSO phase. Interestingly, all of the hydrogen atoms have the same positive charge, suggesting that there is a constant electron shortage in these areas. On the other hand, the carbon atom C6 is the most electron-rich carbon in the molecule and has the highest negative charge, measuring -0.62 in the gas phase and -0.63 in DMSO. Additionally, the oxygen atom O11 has notable negative charges, measuring -0.28 in the gas phase and -0.36 in DMSO. The nitrogen atom N3 also exhibits noticeable positive charges. The MEP analysis reflects these findings. The molecule's reactivity and interactions with other species may be affected by these negative charges, which signify areas of high electron density. Predicting how NHP will behave in different chemical environments and creating molecules with the appropriate characteristics depend on an understanding of the distribution of atomic charges in NHP.

Hirshfeld surface analysis

A graphical representation of the molecular surface has been made feasible by Hirshfeld surface analysis[28], which helps clarify molecular interactions in a crystalline environment by providing more details on weak intra- and intermolecular interactions which impact how molecules are packed in crystals. Figure 6 displays the Hirshfeld surfaces mapped for the NHP with d_{norm} (normalized contact distance) (a), shape index (b), and curvedness (c). By graphing Hirshfeld surfaces over normalized distances (d_{norm}), which ranged from -0.6968 to 0.8868 a.u. and were shown in white, red, and blue in (Fig. 6a), the interatomic short interactions were contrasted with the longer ones. Strong hydrogen bonds and tight interactions are marked by the red patches on the Hirshfeld surface, which are consistent with the higher binding affinity observed in docking tests against targets[29].

Additionally, it is clearly demonstrated by the Hirshfeld surfaces of the molecule that are linked by stacking interactions, as seen in the nearby red and blue triangles (highlighted in red) on the surface of the shape index range of -1.0 to 1.0 (Fig. 6b). Because the OH group is present inside the surface, the following blue triangles are convex regions, while the red triangles are concave locations. The curvedness map (Fig. 6c) for NHP shows a measure of surface texture and has been created within -4 and 0.4 Å.

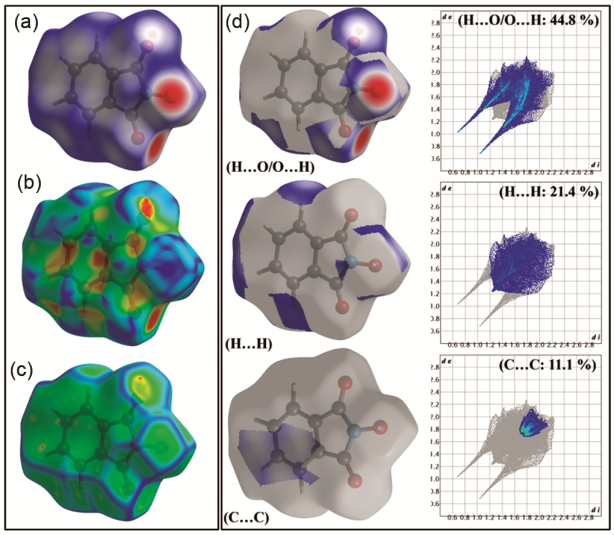

Fig. 6 — (a) d_{norm}, (b) Shape index, (c) Curvedness and (d) Finger print plot Hirshfeld surface interactions with major contribution for N-Hydroxyphthalimide

Regions with high curvedness correspond to sharply curved surface portions, which often divide the surface into square-like domains and reveal interactions between neighboring molecules, whereas smoother areas reflect low curvedness. The large flat region with a blue edge represents the π…π stacking connections.

Fingerprint plots are crucial for identifying interatomic connections and molecular structural information. Two-dimensional fingerprint plots were used to quantitatively characterize the behavior of NHP's intermolecular interactions. H–O/O–H connections account for 44.8% of all surface contacts, making them the most prevalent type of interaction. The H···H (21.4%) and C···C interaction (11.1%) are the second most significant contributors. Conversely, the C···O/O···C and H···C/C···H intercontacts contribute 10.7% and 5.0% respectively, as shown in (Fig. 6d).

Pharmacokinetic properties

Human epithelial colorectal adenocarcinoma cells make up the Caco-2 cell line, which is frequently used as an in vitro model. According to the pkCSM website, a chemical is calculated to have high Caco-2 permeability if its log Papp value exceeds 0.90 cm/s. NHP exhibit high Caco-2 permeability, with a predicted value of 1.167 cm/s. Poor intestinal absorption refers to substances that have an absorption rate of less than 30%. The human intestinal absorption (HIA) of NHP is estimated as 87.2%. A drug molecule's skin permeability[30] (log Kp), an

essential variable in enhancing therapeutic effectiveness, should be more than -2.5 log Kp. The computed log Kp values of NHP have good skin penetrability (-3.2 log Kp) as shown in (Suppl. Table S3). In the low distribution range (compounds with log VDss < -0.15 are considered poorly dispersed, while values > 0.45 indicate wide tissue dispersion), the anticipated steady state volume of distribution (VDss) of NHP was -0.133 log L/kg. Blood-brain barrier (BBB) penetration is restricted, as shown by the intended BBB permeability of -0.268 log BB and agrees well with the standard results[31]. A compound's pharmacokinetic profile, clearance, and possible drug-drug interactions are all greatly influenced by metabolism[30]. NHP is not a substrate of CYP2D6 or CYP3A4, the two main cytochrome P450 isoenzymes that are frequently in charge of drug metabolism, according to the prediction findings. NHP may have a good metabolic safety profile since it is unlikely to undergo substantial metabolism via these pathways and may have a decreased risk of drug-drug interactions.

The estimated NHP total clearance was -0.098 log mL/min/kg, falling within the moderate clearance range. According to this, NHP is probably removed at a reasonable pace, promoting a balanced systemic retention. NHP was also not shown to be a substrate for renal OCT2 transporters, which are frequently implicated in active renal secretion. A negative AMES toxicity test result suggested a minimal risk of genotoxicity and indicated that NHP was non-mutagenic. Additionally, although hERG inhibition is frequently linked to cardiac arrhythmias, NHP was not shown to be an inhibitor of hERG I or hERG II channels, suggesting a lower risk of cardiotoxicity. The estimated oral rat acute toxicity (LD_{50}) of 2.176 mol/kg, indicates a moderate toxicity range. A benign toxicity profile was further supported by the compound's lack of hepatotoxicity and propensity for skin sensitization.

ADMET Profile Comparison of NHP and Anastrozole

Anastrozole is a clinically approved aromatase inhibitor used in the treatment of hormone-dependent breast cancer[32]. The ADMET values for anastrozole shown here are based on the N-(3-bromopropyl) phthalimide that was previously published[33]. In contrast, NHP exhibits improved intestinal absorption, a slightly higher Caco-2 permeability, and a larger unbound proportion, which suggests enhanced free availability. Although NHP has less skin permeability, both show restricted BBB and CNS penetration. NHP exhibits no significant CYP involvement, indicating a lesser risk of interactions between drugs than Anastrozole, which interacts with several CYP450 enzymes. Because NHP is non-mutagenic, non-hepatotoxic, and non-sensitizing, it also has a lower clearance and better toxicity predictions.

Physicochemical properties

Fundamental information about a compound's oral bioavailability and pharmacokinetic behaviour may be gleaned from its physicochemical and drug-likeness characteristics. With a molecular weight of 163.13 g/mol, NHP is drug-like since it is much below the Lipinski threshold of 500 g/mol[34]. The molecule's topological polar surface area (TPSA) was predicted to be 57.61 Å^2, supporting good membrane permeability (TPSA < 140 Å^2 is generally favourable for oral absorption), as shown in (Table 5). Drug-likeness analysis verified observance of the Veber, Egan, and Lipinski's Rule of Five filters. However, it did not meet Ghose's rule, most likely because of flexibility or PSA concerns. After oral administration, there is a modest chance of obtaining excellent systemic exposure, according to the estimated bioavailability score of 0.55.

According to the BOILED-Egg model, which is based on WLOGP and TPSA, NHP is located outside of the yellow yolk, indicating limited BBB penetration, but in the white area, suggesting a high possibility of passive gastrointestinal absorption (Fig. 7). The distribution forecasts (log BB = -0.268,

Table 5 — Physicochemical properties of N-Hydroxyphthalimide

Properties		NHP
Physicochemical properties	Molecular weight (g/mol)	163.13
	No. of H-bond acceptors	3
	No. of H-bond donors	1
	TPSA (Å^2)	57.61
	Fraction Csp3	0.00
Water Solubility	ESOL	-1.74
	ALI	-1.61
	SILICOS-IT	-1.48
Lipophilicity	iLOGP (log P)	1.07
	XLOGP3 (log P)	0.82
	WLOGP (log P)	0.29
	MLOGP (log P)	1.21
	SILICOS-IT (log P)	0.46
Drug-Likeness	Lipinski	Yes
	Veber	Yes
	Ghose	No
	Egan	Yes
	Bioavailability Score	0.55

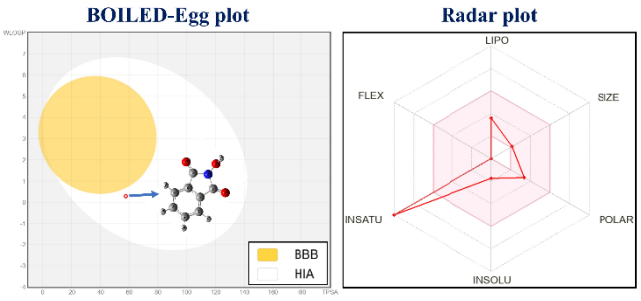

Fig. 7 — BOILED-Egg plot and Radar plot of N-Hydroxy phthalimide

log PS = -2.846) are in agreement with this outcome. NHP also has excellent lipophilicity, polarity, solubility, and molecular size. However, it deviates in saturation (Csp3 = 0.00) and flexibility, according to the bioavailability radar map as shown in (Fig. 7). These findings suggest that NHP has limited CNS penetration, good oral absorption capacity, and generally advantageous drug-like qualities. When NHP and standard medication Anastrozole[32] are compared physicochemically, NHP's molecular weight and TPSA are much lower than Anastrozole's, suggesting a smaller and more flexible structure. Anastrozole continues to be more lipophilic with higher iLOGP and WLOGP values, although NHP exhibits superior aqueous solubility as evidenced by its less negative ESOL and ALI values. Both compounds are in the HIA region according to the BOILED-Egg study, while NHP has a lower potential for BBB penetration. NHP has decreased lipophilicity, size, and saturation parameters, which are consistent with a more drug-like profile, according to radar-plot evaluation.

Molecular docking

Molecular docking is an important computational tool in breast cancer research because it predicts how small compounds or treatment candidates will interact with target proteins implicated in cancer development. Furthermore, molecular docking complements *in vitro* investigations, which aid in the creation of potent anti-breast cancer drugs[35]. In the present study, four major breast cancer associated signaling pathways, the PI3K (Phosphoinositide 3-kinases), Wnt (Wingless and Int-1), MAPK (Mitogen-Activated Protein Kinase), and ER (Estrogen Receptor) were selected based on the KEGG database[36]. The corresponding target proteins were chosen because they are key regulators of these pathways and play crucial roles in breast cancer progression, proliferation, survival, and metastasis[37-40]. Their clinical relevance, frequent dysregulation in breast cancer, and availability of high-resolution crystal structures make them suitable targets for molecular docking studies. Accordingly, the protein structures with PDB IDs 7KBS, 8EXV, 4U7Z, and 3L1S were retrieved from the Protein Data Bank (PDB) and used for docking analysis to identify potential inhibitors capable of interacting with their biologically active residues and suppressing breast cancer related signaling pathways.

Docking analysis revealed that NHP interacts with the ERα binding site[37], suggesting its potential to inhibit receptor activation. This interaction was evaluated using the crystal structure with PDB ID 7KBS, and the NHP–7KBS complex exhibited a binding affinity of -7.1 kcal/mol, indicating a favourable interaction. Less than -3.0 kcal/mol is often regarded as an acceptable binding affinity for a stable association between ligand and protein in molecular docking studies[33]. The binding interactions between NHP and the estrogen receptor (PDB ID: 7KBS) are shown in (Fig. 8a). The complex forms a carbon-hydrogen bond with GLY A:390 at 3.36 Å and a conventional hydrogen bond with LYS A:449 at 2.00 Å. Two π-alkyl interactions are also seen with PRO A:324 (4.14 Å and 4.38 Å) and MET A:357 (5.04 Å). Together, these interactions support the NHP-ER complex's stability. A significant inhibitory interaction was shown by the binding affinity of NHP with PI3K (PDB ID: 8EXV)[40], which has been found to be -6.9 kcal/mol. The binding interactions between NHP and 8EXV are shown in (Fig. 8a), where the complex forms a single carbon-hydrogen bond with ALA A:758 at 4.55 Å.

Furthermore, ARG A:662 (3.39 Å) and PRO A:757 (4.09 Å and 4.64 Å) exhibit two π-alkyl interactions. These interactions show the NHP-PI3K complex's ability to block the PI3K-Akt signalling pathway in breast cancer and help to maintain its stability. According to docking studies, NHP has a significant inhibitory potential and interacts with 4U7Z[39] with a binding affinity of -6.8 kcal/mol. Additional stabilising contacts and one conventional hydrogen bond with MET A:146 (1.88 Å) were revealed by supporting 2D and 3D interaction studies (Fig. 8b). The selected PDB ID: 3L1S[38] was used for the docking studies, which showed that NHP binds efficiently with a binding affinity of −6.7 kcal/mol. Stable binding is further demonstrated by the 2D and

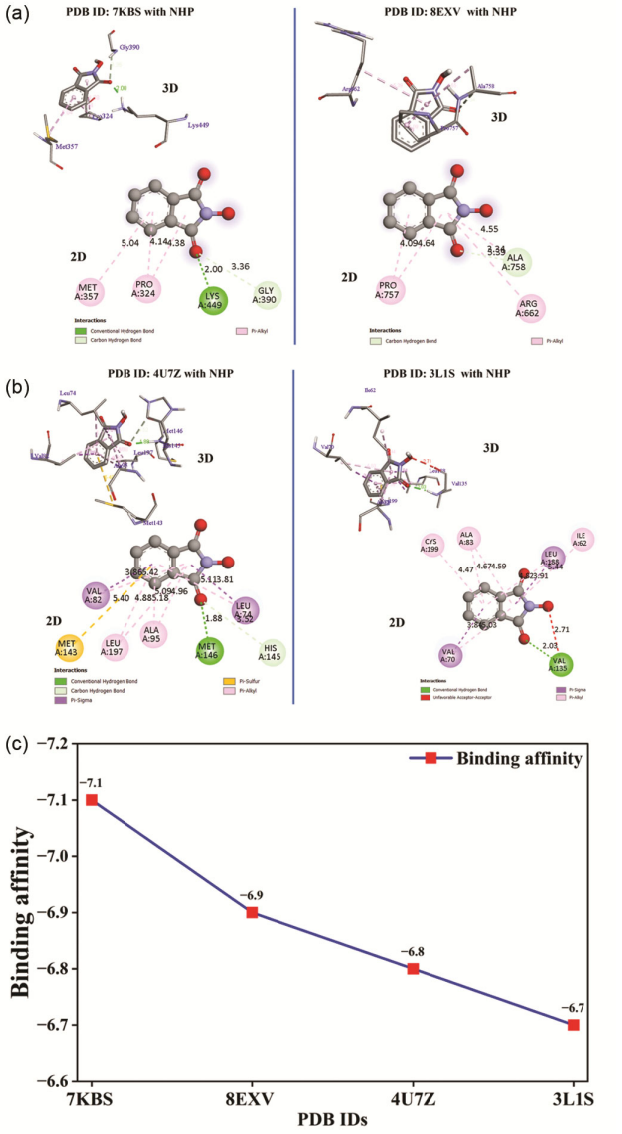

Fig. 8(a) — Molecular docking of 3D and 2D interactions in N-Hydroxyphthalimide with 7KBS and 8EXV proteins, (b) Molecular docking of 3D and 2D interactions in N-Hydroxyphthalimide with 4U7Z and 3L1S proteins, (c) Binding affinity value of N-Hydroxyphthalimide with selected proteins

3D interaction studies (Fig. 8b), which add to the NHP-complex's overall stability. Figure 8c shows the binding affinity for the selected proteins with the ligand. These findings suggest that NHP can effectively block many signalling pathways implicated in tumor growth, cell survival, and proliferation. For the potential therapy of breast cancer, NHP is thus an exciting multi-target agent.

Molecular dynamics simulation and MM/GBSA calculations

To further evaluate the stability of the docked 7KBS–NHP complex, a 100 ns molecular dynamics

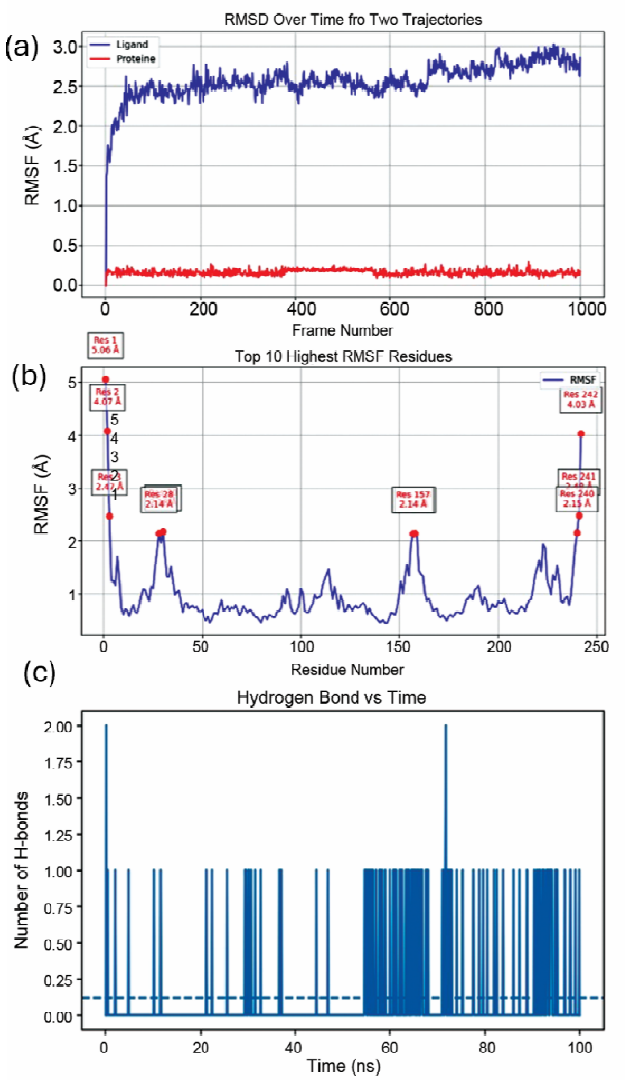

Fig. 9 — Molecular Dynamics Simulations of 7KBS-NHP: (a) RMSD, (b) RMSF, and (c) Hydrogen Bonds

simulation was performed[26,41]. The RMSD profile showed that the complex remained stable throughout the simulation, with the ligand RMSD stabilizing at 2.4–3.0 Å after equilibration and only minor fluctuations in the protein backbone as shown in (Fig. 9a). The RMSF analysis indicated low residue-level flexibility for most amino acids (<1.5 Å), except for slightly higher fluctuations at the terminal and loop regions as shown in (Fig. 9b). Hydrogen bond analysis revealed the intermittent formation of one to two hydrogen bonds during the simulation, supporting sustained protein–ligand interactions (Fig. 9c). In addition, the radius of gyration (R_g) remained stable around 18.16 Å (Suppl. Fig. S3a), while the SASA profile fluctuated around 13,750 Å^2 (Suppl. Fig. S3b) without any significant long-term increase, indicating

maintained compactness and the absence of major unfolding. Hence, these results confirm that the 7KBS–NHP complex remained conformationally stable and structurally compact throughout the 100 ns simulation, supporting the strong binding affinity of NHP toward the target protein.

The MM/GBSA method was used to estimate the binding free energy of the studied complex according to the equation:

$$\Delta G_{bind}=\Delta E_{vdW}+\Delta E_{ele}+\Delta E_{GB}+\Delta E_{SA}$$

where ΔE_{vdW}, ΔE_{ele}, ΔE_{GB}, and ΔE_{SA} represent van der Waals, electrostatic, polar solvation, and non-polar solvation energies, respectively. The entropic term ($-T\Delta S$) was not included in the present study[42,43]. The calculated energy components are summarized in (Table 6).

The calculated MM/GBSA binding free energy was −14.76 kcal/mol, indicating favorable and spontaneous ligand–receptor binding. Among the energy components, van der Waals interactions (ΔE_{vdW} = −21.72 kcal/mol) contributed most significantly to complex stabilization, suggesting that hydrophobic and close-contact interactions dominate the binding process. The electrostatic contribution (ΔE_{ele} = −4.05 kcal/mol) also favored binding, reflecting the presence of attractive intermolecular interactions such as hydrogen bonding and charge-assisted contacts. In contrast, the polar solvation energy (ΔE_{GB} = 14.18 kcal/mol) opposed binding due to the desolvation penalty of polar groups, while the non-polar solvation energy (ΔE_{SA} = −3.17 kcal/mol) provided additional stabilization through hydrophobic effects. Therefore, the MM/GBSA results indicate that the 7KBS–NHP complex is mainly stabilized by van der Waals interactions, supported by electrostatic and non-polar solvation contributions, which is consistent with the docking and molecular dynamics findings.

Cytotoxicity assay

Cell viability assays and morphological studies were employed to thoroughly evaluate the cytotoxic effects of NHP on the breast cancer cell lines MCF-7 and MDA-MB-231[44]. In both cell lines, the data revealed a pronounced dose-dependent decrease in cell viability. The MCF-7 cells showed an IC_{50} value of 14.50 µg/mL (P = 0.007), while the MDA-MB-231 cells exhibited greater sensitivity to NHP, with an IC_{50} value of 16.90 µg/mL (P = 0.002), as shown in (Table 7). These IC_{50} values indicate that the NHP is more effective in both the positive estrogen receptor MCF-7 cell line and the triple-negative MDA-MB-231 cell line. Since both p-values are < 0.05, the results are considered highly statistically significant, confirming the reliability of NHP's cytotoxic activity across both cell lines. Strong cytotoxic ability and the stimulation of pathways for programmed cell death are suggested by the observed decrease in viability. Microscopic examination further supported these findings, revealing notable morphological changes in both cell lines following NHP exposure (Fig. 10). N-(3-bromopropyl)phthalimide, a recently reported halogenyl phthalimide derivative, exhibited IC_{50} values of 16.78 µg/mL against the MDA-MB-231 cell line and 20.60 µg/mL against the MCF-7 cell line[33]. The cytotoxicity results of NHP are comparable to those of the standard breast cancer drug anastrozole[45] (IC_{50} = 18.2 µg/mL) and the recently reported brominated phthalimide derivative, indicating that NHP exhibits comparable or superior anti-breast cancer activity.

Table 6 — Calculated MM/GBSA energy components for the 7KBS–NHP complex in kcal/mol

ΔE_{vdW}	ΔE_{ele}	ΔE_{GB}	ΔE_{SA}	$\Delta G_{MM\text{-}GBSA}$
-21.72	-4.05	14.18	-3.17	-14.76

Table 7 — Mean (%) of cell viability with standard deviation N-Hydroxyphthalimide against MCF-7 and MDA-MB-231 cell lines

Cell line	Concentration of NHP (µg)	Mean (%) of cell viability	IC_{50} and P-value
MCF-7	5	69.79±1.47	14.50 µg/mL
	10	61.99±2.92	(P= 0.007)
	15	54.00±2.05	
	20	35.48±3.22	
	25	22.81±1.75	
MDA-MB-231	5	74.33±4.04	16.90 µg/mL
	10	65.06±3.76	(P= 0.002)
	15	56.15±5.27	
	20	44.39±2.14	
	25	30.66±4.55	

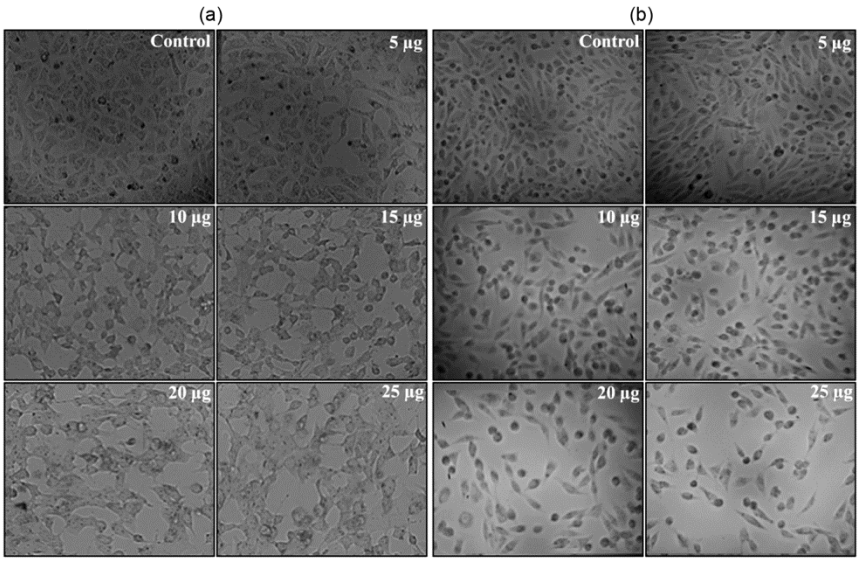

Fig. 10 — Morphological changes image (a) MCF-7; and (b) MDA-MB-231 cell lines with N-Hydroxyphthalimide

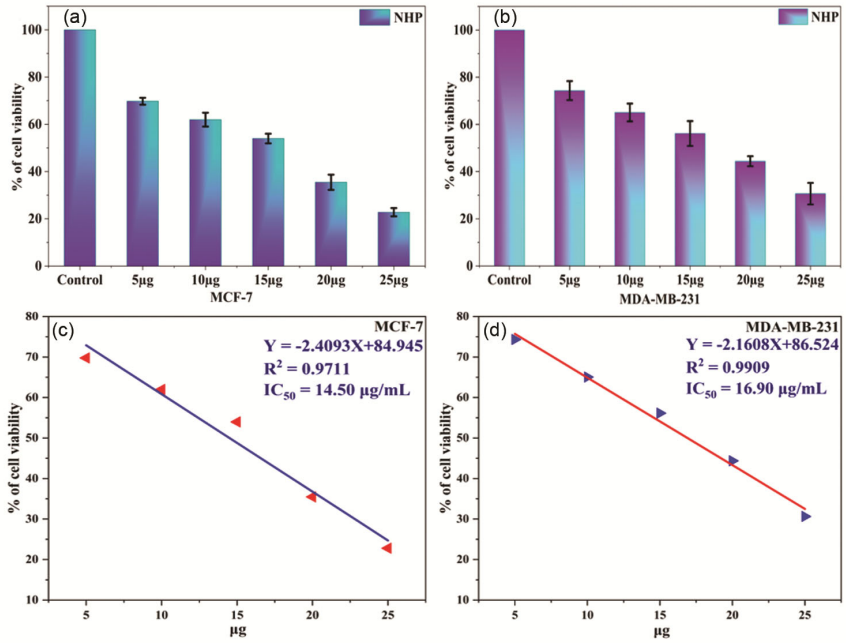

Fig. 11 — (a, b) cell viability % and (c, d) IC_{50} calculation on MCF-7 and MDA-MB-231 cell lines with N-Hydroxyphthalimide

Statistical analysis confirmed the dose-dependent nature of NHP's cytotoxicity, revealing strong linear correlations between NHP concentration and reduced cell viability in both MCF-7 (R^2 = 0.9711) and MDA-MB-231 (R^2 = 0.9909) cells, as shown in (Fig. 11). The steep slopes of the regression equations further emphasized the sharp decline in viability with increasing concentrations. These findings highlight NHP's strong potential to target malignant cells, supporting its promise as a therapeutic candidate for aggressive forms of breast cancer. However, further research is required to explore the therapeutic applications of NHP, particularly through mechanistic studies and *in vivo* models, as well as its role in overcoming drug-resistant cancer types.

Conclusion

N-Hydroxyphthalimide's (NHP) structure was successfully verified using reported bond length and bond angle analysis. IR, Raman, and UV-Vis spectroscopy were among the experimental and theoretical methods that helped to further support its

characterisation. According to TD-DFT analysis, the π→π* transitions of NHP, which are shown as a band at 285.95 nm (experimental) and 298.19 nm and 310.34 nm (gas and DMSO phases, respectively), are responsible for almost 95% of excitation. The chemical activity of the NHP was observed in the HOMO-LUMO energy gap, which was determined to be ΔE = 5.02 eV (gas phase) and 4.86 eV (DMSO phase). MEP analysis indicated neutral areas (green) around the majority of hydrogen atoms, electropositive potential (blue) connected to hydroxyl (OH) group, and electronegative potential (red) surrounding carbonyl (C=O) groups. These results aligned with the Mulliken charge distribution. The characteristics of intermolecular interactions were further emphasised by Hirshfeld surface analysis. According to ADMET profiling, NHP has no appreciable risk of toxicity, including genetic mutation or cardiotoxicity, and is pharmacologically active and orally bioavailable. In addition, it showed a high intestinal absorption rate of 87.2%, minimal BBB permeability, and obeyed Lipinski's Rule of Five. NHP has a substantial binding affinity for the breast cancer target protein 7KBS, according to molecular docking experiments, with the best docking affinity being -7.1 kcal/mol. Consistent RMSD, RMSF, R_g, SASA, hydrogen-bond, and MM/GBSA profiles indicated the 7KBS-NHP complex's stability over the duration of the 100 ns simulation. Strong anticancer activities were also shown by *in vitro* cytotoxicity tests, which showed IC_{50} values of 14.50 µg/mL (MCF-7) and 16.90 µg/mL (MDA-MB-231). By combining experimental spectroscopy, quantum chemical modelling, molecular docking, and cytotoxicity tests, this study positions NHP as a viable platform for next *in vivo* and preclinical anticancer research.

Acknowledgement

The authors would like to thank the management of Kalasalingam Academy of Research and Education for establishing the computational research facility at the International Research Centre (IRC), Kalasalingam Academy of Research and Education, and Jamal Mohamed College for providing the spectrum data. Laboratory of Materials Chemistry and the Living: Activity & Reactivity (LCMVAR), University of Batna 1, Batna, Algeria, for providing computational facilities and support for the molecular dynamics simulations conducted in this study.

Conflict of interest

All authors declare no conflict of interest.

References

1 Khan MM, Yalamarty SSK, Rajmalani BA, Filipczak N & Torchilin VP, Recent strategies to overcome breast cancer resistance. *Crit Rev Oncol/Hematol*, 197 (2024) 104351.

2 Liedtke C, Mazouni C, Hess KR, André F, Tordai A, Mejia JA, Symmans WF, Gonzalez-Angulo AM, Hennessy B, Green M, Cristofanilli M, Hortobagyi GN & Pusztai L, Response to neoadjuvant therapy and long-term survival in patients with triple-negative breast cancer. *J Clin Oncol*, 26 (2008) 1275.

3 Lehmann BD, Bauer JA, Chen X, Sanders ME, Chakravarthy AB, Shyr Y & Pietenpol JA, Identification of human triple-negative breast cancer subtypes and preclinical models for selection of targeted therapies. *J Clin Investig*, 121 (2011) 2750.

4 Chen X, Xu D, Li X, Zhang J, Xu W, Hou J, Zhang W & Tang J, Latest overview of the cyclin-dependent kinases 4/6 inhibitors in breast cancer: the past, the present and the future. *J Cancer*, 10 (2019) 6608.

5 Almeida ML, Oliveira MC, Pitta IR & Pitta MG, Advances in synthesis and medicinal applications of compounds derived from phthalimide. *Curr Org Synth*, 17 (2020) 252.

6 Bodera P & Stankiewicz W, Immunomodulatory properties of thalidomide analogs: pomalidomide and lenalidomide, experimental and therapeutic applications. *Recent Pat Endocr Metab Immune Drug Discov*, 5 (2011) 192.

7 Fernandes GF, Lopes JR, Dos Santos JL & Scarim CB, Phthalimide as a versatile pharmacophore scaffold: Unlocking its diverse biological activities. *Drug Dev Res*, 84 (2023) 1346.

8 Rani R & Granchi C, Bioactive heterocycles containing endocyclic N-hydroxy groups. *Eur J Med Chem*, 97 (2015) 505.

9 Krishnakumar V, Sivasubramanian M & Muthunatesan S, Density functional theory study and vibrational analysis of FT-IR and FT-Raman spectra of N-hydroxyphthalimide. *J Raman Spectrosc*, 40 (2009) 987.

10 Tiron CE, Luta G, Butura M, Zugun-Eloae F, Stan CS, Coroaba A, Ursu EL, Stanciu GD & Tiron A, NHF-derived carbon dots: prevalidation approach in breast cancer treatment. *Sci Rep*, 10 (2020) 12662.

11 Wang M, Zhou A, An T, Kong L, Yu C, Liu J, Xia C, Zhou H & Li Y, N-Hydroxyphthalimide exhibits antitumor activity by suppressing mTOR signaling pathway in BT-20 and LoVo cells. *J Exp Clin Cancer Res*, 35 (2016) 41.

12 Frisch MJ, Trucks GW, Schlegel HB, Scuseria GE, Robb MA, Cheeseman JR, Scalmani G, Barone V, Petersson GA, Nakatsuji H, Li X, Caricato M, Marenich A, Bloino J, Janesko BG, Gomperts R, Mennucci B, Hratchian HP, Ortiz JV, Izmaylov AF, Sonnenberg JL, Williams-Young D, Ding F, Lipparini F, Egidi F, Goings J, Peng B, Petrone A, Henderson T, Ranasinghe D, Zakrzewski VG, Gao J, Rega N, Zheng G, Liang W, Hada M, Ehara M, Toyota K, Fukuda R, Hasegawa J, Ishida M, Nakajima T, Honda Y, Kitao O, Nakai H, Vreven T, Throssell K, Jr. Montgomery JA, Peralta JE, Ogliaro F, Bearpark M, Heyd JJ, Brothers E, Kudin KN, Staroverov VN, Keith T, Kobayashi R, Normand J, Raghavachari K, Rendell A, Burant JC, Iyengar SS, Tomasi J, Cossi M, Millam JM, Klene M, Adamo C, Cammi R, Ochterski JW, Martin RL, Morokuma K, Farkas O, Foresman JB & Fox DJ, Gaussian, Inc., Wallingford CT, 2016. Gaussian 09. 2013 Gaussian 09, Revision A.02, Gaussian, Inc., Wallingford CT.

13 Dennington KR, Millam T & Semichem J, Gaussview, version 5. Semichem Inc., Shawnee Mission, KS. (2009).
14 Becke AD, Thermo chemistry Density-Functional III. The role of exact exchange. *J Chem Phys*, 98 (1993) 5648.
15 Lee C, Yang W & Parr RG, Development of the colle-salvetti correlation-energy formula into a functional of the electron density. *Phys Rev B*, 37 (1988) 785.
16 Jamróz MH, Vibrational energy distribution analysis (VEDA): Scopes and limitations. *Spectrochim Acta - A: Mol Biomol Spectrosc,* 114 (2013) 220.
17 Spackman PR, Turner MJ, McKinnon JJ, Wolff SK, Grimwood DJ, Jayatilaka D & Spackman MA, CrystalExplorer: a program for Hirshfeld surface analysis, visualization and quantitative analysis of molecular crystals. *Appl Crystallogr*, 54 (2021) 1006.
18 Azzam KAL, SwissADME and pkCSM webservers predictors: An integrated online platform for accurate and comprehensive predictions for in silico ADME/T properties of artemisinin and its derivatives. *Kompl Ispolz Min Syra = Compl Use of Min Resour*, 325 (2023) 14.
19 Dallakyan S & Olson AJ, Small-molecule library screening by docking with PyRx. *Chem Biol Meth Protoc*, (2014) 243.
20 Biovia DS, Discovery studio modeling environment, (2017).
21 Dickson CJ, Walker RC & Gould IR, Lipid21: Complex lipid membrane simulations with AMBER," *J Chem Theory Comput*,18 (2022): 1726–1736.
22 Mosmann T, Rapid colorimetric assay for cellular growth and survival: application to proliferation and cytotoxicity assays. *J Immunol Methods*, 65 (1983) 55.
23 Miao FM, Wang JL & Miao XS, N-Hydroxyphthalimide. *Acta Cryst*, 51 (1995) 712.
24 Merrick JP, Moran D & Radom L, An evaluation of harmonic vibrational frequency scale factors. *J Phys Chem A*, 111 (2007) 11683.
25 Shiney A, Jeyavijayan S & Ramuthai M, Spectroscopic, computational investigation, anti-bacterial, docking and cytotoxicity studies on 7-hydroxycoumarin as potent anti-breast cancer agent. *J Indian Chem Soc*, 101 (2024) 101246.
26 Lalitha S, Karthik N, Sumathi S, Srinivasagan G, Messaoudi A, Jeyavijayan S & Vinoth K, Experimental and theoretical investigation of 6-Nitropiperonal through structural, electronic, and biological perspectives. *ChemistrySelect*, 11 (2026) e73247.
27 Kunjumol VS, Jeyavijayan S, Karthik N & Sumathi S, Spectroscopic, computational, docking, and cytotoxicity investigations of 5-chloro-2-mercaptobenzimidazole as an anti-breast cancer medication. *Spectrosc Lett*, 58 (2025) 13.
28 Arunagiri C, Selvakumar S, Jeyavijayan S, Karthik N, Rama I & Subashini A, Synthesis, characterization, and computational study of a benzohydrazide schiff base for electronic and anticancer applications. *Mater Sci Mater Electron*, 36 (2025) 1032.
29 Sumathi S, Karthik N & Jeyavijayan S, Computational and spectroscopic insights into 4-Methoxychalcone as a potential acetylcholinesterase inhibitor: A DFT and Molecular docking approach. *Int J Quantum Chem*, 125 (2025) e70092.
30 Sukumaran S, Zochedh A, Chandran K, Sultan AB & Kathiresan T, Exploring the co-activity of FDA approved drug gemcitabine and docetaxel for enhanced anti-breast cancer activity: DFT, docking, molecular dynamics simulation and pharmacophore studies. *Int J Quantum Chem*, 124 (2024) e27359.
31 Elango AP, Zochedh A, Sultan AB & Sivanandan S, Pharmacokinetics, molecular modeling and in vitro investigation of 4-(2-Amino-2-Carboxyethyl) imidazole against esophagogastric junction adenocarcinoma. *J Comput Biophys Chem*, 25 (2026) 55.
32 Piotrowska I & Piotrowska M, Anastrozole as aromatase inhibitor–new approaches to breast cancer treatment in postmenopausal women. *Nowotwory J Oncol*, 69 (2019) 26.
33 Karthik N, Sumathi S & Jeyavijayan S, Structural characterization, computational analysis, and anti-breast cancer evaluation of N-(3-Bromopropyl) phthalimide. *J Mol Struct*, 1344 (2025) 142958.
34 Chen X, Li H, Tian L, Li Q, Luo J & Zhang Y, Analysis of the physicochemical properties of acaricides based on Lipinski's rule of five. *J Comput Biol*, 27 (2020) 1397.
35 Cava C & Castiglioni I, Integration of molecular docking and *in vitro* studies: A powerful approach for drug discovery in breast cancer. *Appl Sci*, 10 (2020) 6981.
36 Altman T, Travers M, Kothari A, Caspi R & Karp PD, A systematic comparison of the MetaCyc and KEGG pathway databases. *BMC bioinf*, 14 (2013) 112.
37 Hosfield DJ, Weber S, Li NS, Sauvage M, Joiner CF, Hancock GR, Sullivan EA, Ndukwe E, Han R, Cush S, Lainé M, Mader SC, Greene GL & Fanning SW, Stereospecific lasofoxifene derivatives reveal the interplay between estrogen receptor alpha stability and antagonistic activity in ESR1 mutant breast cancer cells. *Elife*, 11 (2022) e72512.
38 Arnost M, Pierce A, Ter Haar E, Lauffer D, Madden J, Tanner K & Green J, 3-Aryl-4-(arylhydrazono)-1H-pyrazol-5-ones: Highly ligand efficient and potent inhibitors of GSK3β. *Bioorg Med Chem Lett*, 20 (2010) 1661.
39 Robarge KD, Lee W, Eigenbrot C, Ultsch M, Wiesmann C, Heald R, Price S, Hewitt J, Jackson P, Savy P, Burton B, Choo EF, Pang J, Boggs J, Yang A, Yang X & Baumgardner M, Structure based design of novel 6, 5 heterobicyclic mitogen-activated protein kinase kinase (MEK) inhibitors leading to the discovery of imidazo [1, 5-a] pyrazine G-479. *Bioorg Med Chem Lett*, 24 (2014) 4714.
40 Hanan EJ, Braun MG, Heald RA, MacLeod C, Chan C, Clausen S, Edgar KA, Eigenbrot C, Elliott R, Endres N & Friedman LS, Discovery of GDC-0077 (inavolisib), a highly selective inhibitor and degrader of mutant PI3Kα. *J Med Chem*, 65 (2022) 16589.
41 Karthik N, Sumathi S, Jeyavijayan S, Lalitha S & Messaoudi A, Integrated theoretical and experimental analysis of 4-amino-N-methylphthalimide: structural, spectroscopic, and anti-breast cancer potential. *SAR QSAR Environ Res*, 36 (2025) 1133.
42 Ylilauri M & Pentikäinen OT, MMGBSA As a Tool to understand the binding affinities of filamin–peptide interactions. *J Chem Inf Model*, 53 (2013) 2626.
43 Wang E, Sun H, Wang J, Wang Z, Liu H, Zhang JZH, Hou T, End-point binding free energy calculation with MM/PBSA and MM/GBSA: Strategies and applications in drug design. *Chem Rev*, 119 (2019) 9478.
44 Karthik N, Sumathi S & Jeyavijayan S, Comprehensive experimental and computational characterization of N-Chlorophthalimide: Structural insights, cancer-protein docking, and cytotoxicity. *Chem Afr*, 9 (2026) 75.
45 Hassan F, El-Hiti GA, Abd-Allateef M & Yousif E, Cytotoxicity anticancer activities of anastrozole against breast, liver hepatocellular, and prostate cancer cells. *Saudi Med J*, 38 (2017) 359.